Applied Catalysis B: Environmental 179 (2015) 213–219

Contents lists available at ScienceDirect

Applied Catalysis B: Environmental

journal homepage: www.elsevier.com/locate/apcatb

Low temperature dry reforming of methane over Pt–Ni–Mg/ceria–zirconia catalysts

Nada H. Elsayed, Nathan R.M. Roberts, Babu Joseph, John N. Kuhn*

Department of Chemical & Biomedical Engineering, University of South Florida, United States

ARTICLE INFO

Article history:
Received 25 February 2015
Received in revised form 7 May 2015
Accepted 9 May 2015
Available online 14 May 2015

Keywords:
Dry reforming
Low temperature
$(CeZr)O_2$

ABSTRACT

Low temperature dry reforming of methane was studied over platinum (0.2–2 wt.%) and/or nickel (8 wt.%) and magnesium (8 wt.%) immobilized onto a ceria–zirconia support. Ceria–zirconia (0.6:0.4) solid solutions were synthesized by precipitation and the metals were loaded by the incipient wetness method. XRD patterns demonstrated that the support was a cubic fluorite structure and Ni and Mg were deposited onto it. Temperature-programmed reduction showed that Pt addition substantially decreased the reduction temperature and the impact became less prominent with increasing Pt loading. The Ni–Mg/$(Ce_{0.6}Zr_{0.4})O_2$ had the highest number of basic sites and the amounts decreased with the addition of platinum. The lowest CH_4 and CO_2 conversion (X_{10}) temperatures were achieved at 454 °C and 437 °C, respectively, using a 0.5% Pt–Ni–Mg/$(Ce_{0.6}Zr_{0.4})O_2$ catalyst. This catalyst was optimum because it balanced between the enhanced reducibility and decreasing number of basic sites, which both occurred with increasing Pt loading. Dry reforming experiments also indicated that Pt decreased the reaction onset temperature for methane and CO_2 and correlated to a slight decrease in the H_2:CO ratio (though still higher than for the 0.5% Pt–$Ce_{0.6}Zr_{0.4}O_2$ control catalyst). Steady-state reaction experiments were conducted between 430 and 470 °C for the best catalyst and the results showed TOFs increasing from 2.69 to 4.74 s^{-1} with increasing temperature and minimal deactivation when left on stream for 100.5 h. A comparison to literature indicates that the Pt/Ni/Mg/$Ce_{0.6}Zr_{0.4}O_2$ catalyst has among the highest activities, especially if Ir and Rh catalysts are not included.

1. Introduction

Fossil fuels are a finite resource and the world's energy demands are constantly increasing. Alternative fuel sources are no longer optional, but are now a necessity. Dry reforming of methane (DRM) has been extensively studied in recent years [1–6]. The process can produce syngas at a H_2:CO ratio of 2:1 which is ideal for Fischer Tropsch Synthesis (FTS) and methanol synthesis, when combined with other reactions, such as steam reforming [2,7,8] or the water–gas shift (WGS). As a greenhouse gas, methane is 20 times more powerful at trapping heat than carbon dioxide, which makes it considerably harmful to the atmosphere. According to the EPA [9], 29% of methane emissions come from natural gas and petroleum, whereas enteric fermentation (25%), and landfills (18%) also account substantially. The remaining 28% are emitted through various processes such as coal mining and wastewater treatment. These are also under-used sources of methane, which either contain or could be combined with carbon dioxide and other oxidants for conversion processes. For example, biodegradable municipal waste in landfills produces landfill gas (LFG, comprised of roughly equal amounts of methane and carbon dioxide) and the EPA is currently limiting methane emissions from landfills [10]. In addition, biogas can be generated from the anaerobic digestion of biomass and syngas can also be obtained using natural gas in combination with flue gas from fossil fuels. The underlying theme of these approaches is dry reforming.

The dry reforming process utilizes carbon dioxide to help reform methane and obtain hydrogen and carbon monoxide as products through the following reaction:

$$CH_4 + CO_2 \rightarrow 2H_2 + 2CO (\Delta H^\circ = 247.3\ kJ/mol)$$

The produced syngas can then be utilized for fuel synthesis of hydrocarbon and oxygenate fuels and chemicals when combined with steam reforming or the WGS reaction. The endothermic dry reforming reaction readily occurs at high temperatures [1]. However, that also adds to the overall cost of the process on an industrial scale, as methane is often parasitically combusted to generate the heat. The DRM reaction is thermodynamically predicted to not

* Corresponding author. Tel.: +1 813 974 6498.
E-mail address: jnkuhn@usf.edu (J.N. Kuhn).

http://dx.doi.org/10.1016/j.apcatb.2015.05.021
0926-3373/

occur at temperatures below 350 °C with coking being the only possible pathway at such low temperatures [7,11]. Low temperature dry reforming of methane could reduce the cost making it industrially more viable. This work demonstrates low temperature reforming activity, stability, and the components required for an active catalyst.

The reforming temperature is affected by both the support and the catalyst used. Many supports have been investigated for dry reforming of methane including silica, alumina, $(Ce,Zr)O_2$ and perovskites [6,12,13]. For this work, a mixed ceria–zirconia oxide support $(Ce_{0.6}Zr_{0.4})O_2$ was chosen for a variety of reasons. Literature shows that ceria has a high oxygen storage capacity (OSC) which is useful for the reaction in enhancing the reducibility within the fluorite lattice [14]. The ratio chosen for this work was also shown to have the highest catalyst activity and stability versus other compositions [13,15]. Adding zirconia which has a smaller ionic size, helps create a lattice strain which in turn causes high oxygen mobility that help improve the redox properties [16,17]. In addition, $(Ce,Zr)O_2$ is thermally stable at high temperatures [13,14]. The addition of zirconia to ceria also helps to shift the oxygen vacancies to the more stable surfaces (1 1 1) and (1 1 0). This oxygen shift aids in moving the reduction equilibrium to the right by utilizing bulk oxygen which in turn significantly favors bulk reduction [18].

Nickel-based catalysts have been widely investigated for dry reforming of methane due to the abundance of nickel, high activity and the economically feasible cost [4,7,19–21]. However, they have a major disadvantage of rapid deactivation and coke formation especially in biomass feedstock due to the presence of sulfur-containing impurities [7,21,22]. Adding a small amount of noble metal such as platinum can help decrease coking and enhance catalytic stability and activity [13,17,23]. Adding platinum also helps reduce ceria to Ce^{3+} and create oxygen vacancies [24]. Moreover, Pt, even in low loadings, could provide active sites for the conversion. In addition, adding MgO can help to increase the Lewis basicity of the support [7,25]. This solid solution enhances CO_2 adsorption by adding stability to the Ni crystallites which can reduce carbon deposition from CO disproportionation [7,26].

The main goal of this work was to examine the effects of different platinum loadings on structure, properties, and dry reforming performance of metal based catalysts immobilized onto a ceria–zirconia support. The addition of a precious metal in low loadings to a Ni-based catalyst is a viable way to achieve low temperature reforming catalysis. The support was synthesized via co-precipitation and metals were loaded via wetness impregnation. Reduction experiments (TPR) showed that adding Pt onto the catalyst favorably decreased the reduction temperature but the impact became less prominent with increasing Pt loading. In addition, CO_2 temperature-programmed desorption (TPD) studies showed that the addition of Ni and Mg increased catalyst basicity, but the further addition of Pt led to a slight decrease in basic sites. The results of this study demonstrate that the balance between reducibility and basic sites are the influential factors in enhancing the low temperature dry reforming activity in this catalyst system and lead to high activity. The study also demonstrates improvements beyond both the control catalysts that do not contain either Ni and Mg or Pt. The catalysts in this study has among the highest activity for low-temperature (compared at $T = 450$ °C) dry reforming in the literature for catalysts not containing Rh or Ir.

2. Experimental

2.1. Materials and synthesis

Ceria–zirconia was prepared via the co-precipitation method as reported by Rossignol et al. [27] in a ratio of 0.6:0.4. The $(Ce_{0.6}Zr_{0.4})O_2$ support was made in batches of 12 g by weighing 8.7 g of the cerium precursor $Ce(NO_3)_3{\cdot}6H_2O$-(99.5% pure; Alfa Aesar) and 3.3 g of zirconium precursor $ZrO(NO_3)_2{\cdot}H_2O$-(99.9% pure; Alfa Aesar). The precursors were then dissolved in 150 mL of deionized water in a large beaker. About 75 mL of ammonium hydroxide (27% w/w NH_3; Mallinckrodt Chemicals) was added to the beaker in 10 mL increments to precipitate the precursors until a clear liquid layer was visible on top of the beaker indicating complete precipitation. The mixture was vacuum filtered and then re-dissolved in 0.25 M NH_4OH solution. The solution was vacuum filtered a second time. The filtrate was dried in an oven at 60 °C for 1 h, then 120 °C for 12 h. Finally, the powder was calcined at 800 °C for 4 h.

Nickel (8% by mass), magnesium (8% by mass), and platinum were loaded on the support via incipient wetness impregnation. Platinum was loaded at 0.2%, 0.5%, 1% and 2% by mass ratio. The nickel precursor $Ni(NO_3)_2{\cdot}6H_2O$ (99.9985% pure; Alfa Aesar), the magnesium precursor $Mg(NO_3)_2{\cdot}H_2O$ (99.999% pure; Alfa Aesar) and the platinum precursor $H_2PtCl_6{\cdot}6H_2O$ (Sigma–Aldrich) were used for the metal loadings. The desired amount of each metal was weighed and all of the precursors were dissolved in an appropriate amount of deionized water (1–2 mL) in one beaker. The solution was then added drop wise onto the support until incipient wetness. The powder was then dried in an oven for 2 h at 120 °C to remove any volatile components and evaporate the water. The process was repeated until all the solution was added. After the final drying, the powder was calcined at 600 °C for 3 h. A control sample that contained no nickel and magnesium was synthesized the same way as mentioned above.

2.2. Catalyst characterization

The synthesized catalyst was characterized using TPR, XRD, N_2 physisorption, and CO_2-TPD. Temperature-programmed reduction (TPR) was done using a Cirrus MKS mass spectrometer (MS) connected in-line with the reactor containing 50 mg of calcined catalyst. The catalyst was loaded between two layers of quartz wool. The reactor was then positioned inside a Thermoscientific Thermolyne tube furnace and high temperature glass wool was added to insulate the top of the furnace. Feed gases were controlled using Alicat Scientific mass flow controllers. All of the gas feed and outlet were wrapped in heating tape to prevent condensation prior to entering the MS. The furnace temperature was controlled using a Eurotherm 3110 PID controller. Each catalyst sample was pretreated under an ultra-high purity (UHP, Airgas) helium flowrate of 50 sccm at 110 °C for 30 min using a ramp rate of 10 °C/min. The sample was then allowed to cool to 50 °C and then the gas flow was switched to 5% H_2/He (50 sccm). The sample was then heated at a ramp rate of 10 °C/min to 900 °C and held for 30 min. For the data analysis, calibration curves were measured to calculate the ionization factors.

X-ray diffraction (XRD) was done to determine the crystal structure using a Bruker AXS operating with a Cu Kα source at 40 kV and 40 mA. The data were obtained using a (2θ) angular range of 15–80°. The step size was 0.02° and the dwell time was 3 sec for each step.

BET surface areas and pore volumes were obtained using a Quantachrome Autosorb-IQ. Each experiment was done using 50 mg of catalyst. The sample was first pretreated at 120 °C for 2 h. The sample was then loaded in a small-bulb 6 mm quartz cell. Then, the sample was backfilled with He and outgassed under vacuum for 1 h. The surface area values were obtained by fitting the data to BET isotherm in the P/P_0 range of 0.05–0.33 using N_2. The pore volume is reported at P/P_0 of ~1. The BJH method was used to determine the average pore size.

CO_2 temperature-programmed desorption (CO_2-TPD) studies were done to determine the catalyst basicity using the same

Table 1
Surface, Bulk properties, reduction temperatures, and CO_2 adsorption data.

Sample	Notation	S_{BET} (m^2/g)	Pore volume (cc/g)	Pore diameter (nm)	Reduction temperature (°C)	Amount CO_2-desorbed ($\mu mol/g_{cat}$) (temp 50–400 °C)
$Ce_{0.6}Zr_{0.4}O_2$	CeZr	152[a]	0.35 [a]	14.1[a]	618	0.38
0.5% Pt–$Ce_{0.6}Zr_{0.4}$ O_2	0.5Pt/ CeZr	70	0.16	11.4	196–480	0.71
$Ce_{0.6}Zr_{0.4}O_2$–8Ni8Mg	0Pt	40	0.10	11.4	382	1.40
0.2% Pt–$Ce_{0.6}Zr_{0.4}O_2$–8Ni8Mg	0.2Pt	30	0.08	11.4	283	1.29
0.5% Pt–$Ce_{0.6}Zr_{0.4}O_2$–8Ni8Mg	0.5Pt	31 [a]	0.07 [a]	11.6 [a]	248 [a]	1.30
1% Pt–$Ce_{0.6}Zr_{0.4}O_2$–8Ni8Mg	1Pt	34 [a]	0.09 [a]	11.3 [a]	247 [a]	1.07
2% Pt–$Ce_{0.6}Zr_{0.4}O_2$–8Ni8Mg	2Pt	22	0.05	11.4	242	0.98

[a] The average of two different samples is reported.

system already described in the TPR section. The catalyst (75.5 mg) was initially reduced at a temperature of 300 °C in a 5% H_2 in He gas mixture and held at the reduction temperature for 1 h. The catalyst was then cooled under He only until a temperature of 50 °C was reached. After the temperature stabilized, a 10% CO_2 in He was introduced to the catalyst and flown for 30 min. The catalyst was then purged by flowing He only for another 30 min. The temperature was then increased to 800 °C at a ramp rate of 10 °C/min and held for 10 min.

2.3. Catalytic testing

Reactions experiments were done in a quartz u-tube microreactor with an internal diameter of 4 mm. All reactions were done at atmospheric pressure using 75.4–75.7 mg of catalyst. The same system described in the TPR section was utilized. The catalyst was first reduced at a temperature of 300 °C in a 5% H_2 /He for 1 h. For the temperature-programmed reactions (TP-rxns), the temperature was then decreased in He (50 sccm) to 200 °C and then reforming gas mixture was introduced once this temperature was reached. Methane and carbon dioxide, (both 99.999% pure from Airgas), were introduced in a 1:1 ratio with a total composition of 14% reactants in He gas (44 sccm total flow). The temperature was then increased to 900 °C at a 10 °C/min ramp rate and held there for 30 min. The gas hourly space velocity (GHSV) was maintained constant at 68,000 h^{-1} for all reactions unless otherwise stated. Methane and carbon dioxide conversions were calculated using the following formulas:

$$CH_4 conversion = 1 - \frac{(mol\ out)}{(mol\ in)}$$

$$CO_2 conversion = 1 - \frac{(mol\ out)}{(mol\ in)}$$

Steady-state data were collected using a similar procedure. After the reduction and cooling to 200 °C in He, the reforming gas mixture was introduced and the temperature was raised to 470 °C. Once steady-state was reached, the temperature was decreased by 10 °C and this was repeated until 430 °C. TOFs were calculated from the steady-state CO_2 conversion at the various temperatures, using the amount of CO_2 desorbed from the CO_2 TPD to estimate the number of sites. The Weisz–Prater criterion was calculated to be $\sim 10^{-3}$ which is $\ll 1$ indicating that there were no internal diffusion limitations. External mass transfer limitations were determined to be negligible at the GHSV used (determined by testing a series of GHSVs). Regardless of GHSV for the 0.5Pt catalyst, the H_2:CO ratio was largely independent of it at $T = 450$ °C and was ~0.27–0.30, as determined by a separate set of experiments. In a final experiment for the 0.5Pt catalyst, its stability was tested during an extended time-on-stream (TOS) of 100.5 h.

A temperature-programmed oxidation study was done following each of the TP-rxn experiments and selected steady-state experiments to quantify the presence of carbon deposits. After reaction experiments, the catalyst was rapidly cooled to 60 °C under He (50 sccm). A 10% oxygen in He gas mixture (50 sccm total) was then introduced to the catalyst. The temperature was then increased to 900 °C using a 10 °C/min ramp rate and held for 1 h. No coke formation was detected from any of the samples.

3. Results and discussion

For this work, a series of catalysts were synthesized on a $Ce_{0.6}Zr_{0.4}O_2$ support. The synthesized catalysts were 8% Ni 8% Mg–$Ce_{0.6}Zr_{0.4}O_2$ (0Pt), 0.5% Pt–$Ce_{0.6}Zr_{0.4}O_2$ (0.5Pt/CeZr), 0.2% Pt–8Ni8Mg–$Ce_{0.6}Zr_{0.4}O_2$ (0.2Pt), 0.5% Pt–8Ni8Mg–$Ce_{0.6}Zr_{0.4}O_2$ (0.5Pt), 1% Pt–8Ni8Mg–$Ce_{0.6}Zr_{0.4}O_2$ (1Pt), 2% Pt–8Ni8Mg–$Ce_{0.6}Zr_{0.4}O_2$ (2Pt). The baseline sample (Ni and Mg, but not Pt) was used for tri-reforming by our group in a previous study [15], which optimized the Ni and Mg loadings and the Ce:Zr ratio for activity and stability purposes. The notation used for each catalyst from this point forward is included in Table 1.

3.1. Characterization

The effect of metal immobilization on the surface area of the support and the pore volumes was examined by N_2-physisorption and is reported in Table 1. The synthesis method and ceria to zirconia ratio have a large effect on the surface area of the support which is the reason the literature values range from 35 to149 m^2/g [2,13,15,28,29]. Previously published studies have shown that high ceria content has been identified to cause pore blockage of the zirconia and decrease the overall surface area [2,27,30].

For this work, the oxide support had the highest surface area of 146 m^2/g which is similar to reported values in literature [13]. The surface areas decreased as the metals were loaded as well as the measured pore volumes as reported in Table 1. A similar decrease upon metal loading was observed in literature and it was attributed to the pore blockage and sintering by the loaded metals [15,31,32]. The decrease in the pore diameters upon loading also contributed to the decrease in pore volume. The BJH pore size distribution curves for all samples is included in the supporting information (Fig. S1). Whereas, the main pore diameter decreases its width upon loading, the smaller pores tended to be completely blocked. This result is in agreement with the change in surface areas and pore volumes between the support alone and the supported catalysts.

XRD was conducted to ensure that the support is correctly synthesized and the metals are loaded onto the surface. The results are shown in Fig. 1. The $(Ce_{0.6}Zr_{0.4})O_2$ pattern showed no evidence for the monoclinic phase which are characteristic of ZrO_2. However, the pattern is consistent with a cubic fluorite structure as is previously reported in literature [15,28,33]. This finding suggested that the ZrO_2 is incorporated into the CeO_2 lattice. As reported previously [34], the asymmetry of the diffraction lines also suggested the presence of multiple ceria–zirconia solid solution phases of various compositions. The third diffraction pattern (0Pt) showed the support with only nickel and magnesium loaded. NiO and MgO

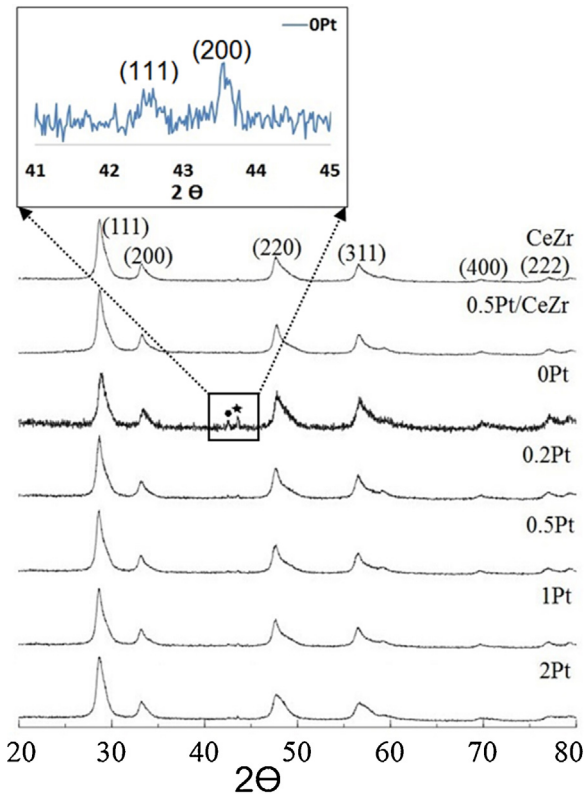

Fig. 1. XRD pattern of catalysts, where (⋆) represents the (1 1 1) and (●) represents the (2 0 0) NiO and MgO diffraction lines as shown in the insert for the 0Pt sample. The Miller indices refer to the cubic fluorite (Ce,Zr)O_2 phase (except for the insert).

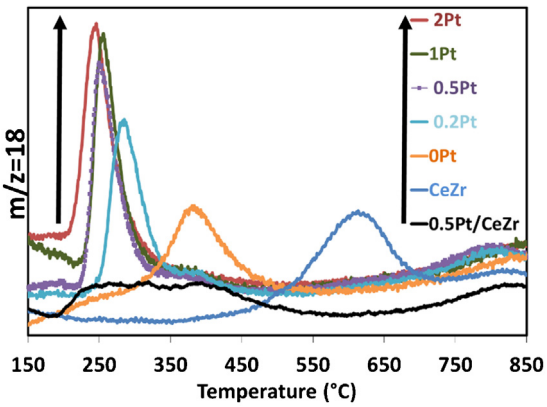

Fig. 2. TPR profiles of catalysts, indicative arrows show signal to legend trend of the curves.

diffraction lines can be seen around a 2θ of 42–44° proving that the metals are deposited onto the support. The diffraction patterns of the catalysts with different platinum loadings are also shown in Fig. 1. Since the platinum content is low and is most likely highly dispersed on the support, no significant diffraction lines related to platinum are observed in the diffraction patterns. This result agreed with other groups who have made similar observations [32]. It is unclear whether the Pt is evenly distributed across the surface or is preferentially adsorbed the support or the (Ni,Mg)O phase. In addition, post-reaction and post-reduction XRD patterns were obtained on select catalysts and there were not any observable diffraction shifts or changes.

TPR was utilized to characterize the catalyst's reducibility. In addition, it also shows how different species within the catalyst interact with each other [15,35]. The results of the temperature-programmed reduction experiments on the calcined materials can be seen in Fig. 2 and are summarized in Table 1. The support alone had a reduction peak at 618 °C, which was consistent [36] with previous findings. Adding Ni and Mg shifted the reduction peak to 382 °C. This result agreed literature that nickel helps the ceria to become more reducible by producing mobile oxygen [33]. However, the nickel-based catalyst without any platinum content reduced at a much higher temperature than catalysts with platinum. The addition of platinum helped further decrease the reduction temperature significantly at first with smaller shifts in reduction as Pt content increased. The catalyst that did not have any nickel or magnesium but had platinum displayed a small but very wide reduction peak that ranged from 196 °C to 490 °C. This implies that the platinum interaction with the support has a significant effect on increasing the reducibility of the ceria support as well [37–39]. Platinum helps reduce the oxide phases through its affinity to facilitate dissociative hydrogen adsorption. Hydrogen has been identified to adsorb and dissociate on the surface of the platinum whereby it spills over to the entire surface of the ceria [38]. The impact of Pt becoming less prominent with increasing Pt loading likely occurred because the dispersion of the Pt crystallites probably increased with loading.

There is no general consensus in literature as to which species contributes to each of the two main reduction peaks whether it is as a result of the support or NiO. Kumar et al., Walker et al., and Diskin et al. [13,15,40] agreed that the low temperature reduction peak (600 °C and below) is attributed to the NiO species. Dong et al., Escritori et al. and Roh et al. [20,28,33] attributed the low temperature reduction peak to the surface region of cerium oxide that is promoted by weakly bound loaded nickel. Whereas the higher temperature reduction peak (800–900 °C) was attributed to the bulk ceria promoted by strongly bound NiO species. Literature has shown unsupported NiO to have a first early reduction peak in the 400–430 °C range [28,33]. For this work, it was determined that the initial reduction temperature is most likely as a result of the weakly bound NiO species. The second reduction peak is most likely attributed to the NiO species with strong interaction with the support [20,28,33].

From the reduction profile of (CeZr)O_2, it is clear that the support was reduced in agreement with others [2,24,41]. Addition of NiO onto the support caused a decrease in the reduction temperature to 382 °C which is below the previously reported NiO reduction temperature of 405 °C [33]. Addition of platinum further decreased the reduction temperature, which corroborated with literature [2,24,42]. Based on the trend and the width of the peaks in the reduction profiles, it is believed that the support is what is mainly getting reduced. However, the metal oxide materials also get reduced which is evident by the sharpness of the reduction peaks for the metal loaded samples. As a result of the metal interaction with the support, they help lower the reduction temperature of the support [32,42]. This increase in the supports' reducibility occurs as a result of increasing the mobile oxygen.

Temperature-programmed desorption of CO_2 experiments done on the reduced catalysts are provided in the supporting information (Fig. S2) and the results are summarized in Table 1. All metal supported catalysts displayed a strong initial peak in the range <200 °C and had a large profile that extended to about 400 °C. The support alone only had a double peak from 100–200 °C. This result is consistent with findings in literature [33] which suggest that ceria adds medium basic sites as a result of its large OSC which aids in capturing and releasing oxygen. Adding NiO and MgO improved the basicity of the support as the amount of CO_2 adsorbed increased from 0.38 $\mu mol/g_{cat}$ in the support only sample to 1.40 $\mu mol/g_{cat}$ in the catalyst with nickel and magnesium [7]. This finding was expected because Mg was anticipated to add surface basicity. This

Table 2
Temperature-programmed reaction results for the various catalysts.

Sample	X_{10} CH_4 temperature (°C)	X_{50} CH_4 temperature (°C)	X_{10} CO_2 temperature (°C)	X_{50} CO_2 temperature (°C)	H_2:CO (@450 °C)
CeZr	828	n/a	787	n/a	n/a
0.5Pt/CeZr	504	641	759	810	0.23
0Pt	762	848	742	813	n/a
0.2Pt	464	611	450	586	0.35
0.5Pt	454	603	432	578	0.30
1Pt[a]	479	608	467	590	0.21
2Pt	493	613	479	595	0.22

[a] Reporting the average values of two samples.

effect was greater than the effect of adding platinum alone to the support which only yielded an adsorbed amount of 0.71 μmol/g_{cat}. This decrease in adsorbed CO_2 amount with Pt loading is correlated to the surface area and pore volume decreases reported in Table 1. Literature attributes the lower CO_2 desorption for the platinum catalysts to the dense nature of the oxygen vacancies [43].

3.2. TP-Rxn results

Both 10% conversion and 50% conversion temperatures of CH_4 and CO_2 are reported in Table 2 as X_{10} and X_{50}, respectively. Results showed 10% methane conversion was achieved at 828 °C using only the ceria–zirconia support. In addition, 10% carbon dioxide conversion was achieved at 787 °C. Adding nickel and magnesium effectively lowered the conversion temperature to 762 °C and 742 °C for methane and carbon dioxide, respectively. The addition of platinum further decreased the conversion temperature. Adding Pt alone to the support without Ni and Mg significantly decreased the X_{10} and X_{50} temperatures. However, adding Pt along with Ni and Mg gave the lowest X_{10} and X_{50} temperatures as reported in Table 2. The 0.5Pt catalyst showed the most desirable results with an X_{10} for methane at 454 °C and for carbon dioxide at 437 °C. The equilibrium carbon dioxide conversion, in the absence of coke formation, of 10% would occur at approximately 400 °C [11]. High carbon dioxide conversions, relative to methane conversions for a given sample, occurred due to the reverse WGS (rWGS).

The H_2:CO ratio was highest in the catalysts with 0.2Pt and 0.5Pt as reported in Table 2. From the trend, it is evident that the H_2:CO ratio decreases with increasing platinum content. This trend is likely a result of decreased platinum dispersion as the amount of platinum increases. In addition, H_2:CO was not close to the desired 1:1 ratio. The low H_2:CO ratio is attributed to the rWGS simultaneously occurring at the low temperatures used for this work. This is further proved by a visible water signal in the MS output data and consistent with other published works [2] and with the thermodynamics. Other published works have shown a H_2:CO ratio of 0.05–0.3 for low temperature dry reforming of methane as well [3]. In the post-reaction TPOs, carbon dioxide produced from coke combustion was not detected in any experiment. This finding is consistent with that the base catalyst (0Pt) was optimized (in terms of Ni and Mg loading and Ce:Zr ratio) for anti-coking behavior in a previous study [15] and the water formation from the rWGS because water would be better at oxidizing coke deposits than CO_2.

The activity trends as a function of two descriptors (peak reduction temperature and number of basic sites) for all catalysts examined in this study is shown in Fig. 3. The relative activity correlates to the marker size, with larger markers indicating more activity (as defined as inversely proportional to the X_{10} temperature, Table 2). Compared to the catalyst without Pt (0Pt), the decrease both in the amount of basic sites and peak reduction temperatures correlated to increasing Pt amounts. Thus, one of the intermediate Pt loadings (i.e., the 0.5Pt sample) yielded the highest dry reforming activity. Since the optimal Pt loading was low, the high platinum dispersion also likely aided in the high activity. High

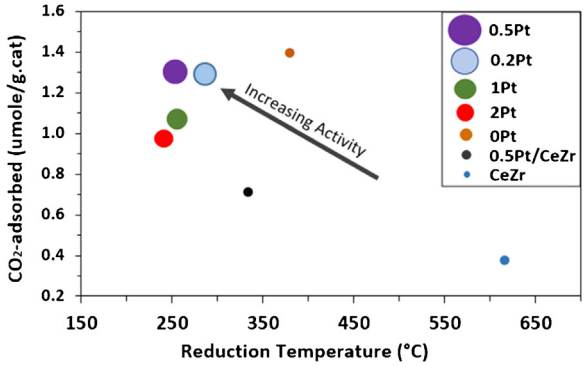

Fig. 3. Dry reforming activity trends. Adding Pt increased the number of basic sites leading to higher activity for dry reforming. Note that the size of the circles is directly proportional to the activity.

Pt dispersion has been identified to help improve dry reforming activity [2,32,44].

3.3. Steady-state reaction results

Steady-state experiments were conducted using the 0.5Pt catalyst, with the same feed and space velocity as the TPRxns. First, an isothermal (T = 450 °C) stability (TOS = 100.5 h) test is described. During the initial heating in the presence of reactants, results showed methane (X_{10}) conversion at 444 °C (10 °C different than shown in Table 2) and carbon dioxide (X_{10}) conversion at 430 °C (2 °C different than shown in Table 2). At T = 450 °C, the catalyst showed slight deactivation (CH_4 conversion only) over the course of the 100.5 h on stream (Fig. 4). The average H_2:CO ratio during this TOS was 0.32 and this result agreed with the temperature-programmed value (0.30) for this sample (Table 2). Despite the lengthy TOS, this catalyst showed no coking as measured by a post-reaction TPO (Fig. 4).

In a separate experiment, turnover frequencies (TOFs) were obtained for the steady-state CO_2 conversion (normalized by the total CO_2 amount desorbed) of the same, most active sample (0.5Pt)

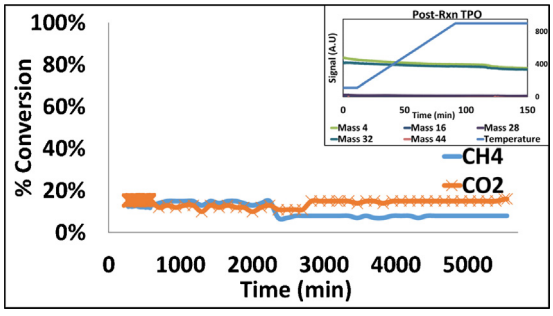

Fig. 4. CH4 and CO2 conversion from 100.5 h stability test and insert shows post-test TPO with no coking present.

Table 3
Activation energies of different metal-based catalysts.

Catalyst	Apparent activation energy (kcal/mol)		Conditions[a]	Reference
	CH_4	CO_2		
0.5Pt	18.5	14.8	430–470 °C	This study
5% Ni/CaO–Al_2O_3	25.5	23.6	620–690 °C	[4]
Ni/γ-Al_2O_3	12.2	13.4	500–700 °C	[21]
CeO_2–ZrO_2	24.1	n/c	400–630 °C	[29]
Ni(100)	17.7 ± 2.4	n/c	171–253 °C P = 4.4 mbar	[45]
Ni/CZ	16–18.9	n/c	550–840 °C	[46]
Pt/ZrO_2	n/c	19.8	600 °C P = 25 kPa	[47]
0.2Pt–15Ni/CaO–Al_2O_3	26.6	16.9	580–620 °C	[48]

n/c refers to not calculated.
[a] Pressure is 1 atm unless otherwise noted. n/c refers to not calculated.

in the temperature range of 430–470 °C. At the lowest temperature (430 °C), the TOF was 2.69 s^{-1}. The TOF increased with increasing temperature with values of 3.17 s^{-1}, 3.50 s^{-1}, 4.22 s^{-1}, and 4.74 s^{-1} at respective temperatures of 440 °C, 450 °C, 460 °C, and 470 °C. Literature reported comparable TOF for 3.8% Rh/SiO_2 catalyst where the values were between 1.5–3.6 s^{-1} at 450 °C and 0.1 MPa depending on the space [11] velocity. The TOFs were calculated from the CO_2 conversion using TPD site density (assuming 1:1CO_2:site). Since it was assumed constant, the rate of CO_2 conversion is TOF × site density. The methane rates would be slightly lower since the methane conversion was lower than CO_2 conversion, due to the reverse water–gas shift reaction.

The apparent activation energies were calculated to be 18.5 and 14.8 kcal/mol from the respective CH_4 and CO_2 conversion data and these value were consistent with the literature (Tables 3 and 4). A comparison of different catalysts and their respectively reported activation energies is included in Table 3. Qualitatively, lower apparent activation energies for CO_2 as compared to CH_4 makes sense since multiple pathways (dry reforming and rWGS) are more likely to exist and corroborated with the results of Table 3.

As shown in Table 4, activation energies and turnover frequencies from a number of studies are compared. Ni and Pt are included since they are used in the current study and Rh and Ir are included because they are the most active. Since SiO_2 in general is an inert supports, its use in supported catalysts are included as well as the support which yields the most active catalyst for each immobilized metal. The various activation energies and original conversion studies are available as the reference column. The actual TOF values are the corrected values published by Bradford and Vannice [7]. In general, the TOF values were corrected using the reported activation energies and concentration dependencies (as described in the footnotes of Table 4) to conditions of their studies (T = 450 °C, $P_{CO2} = P_{CH4}$ = 195 Torr).

Table 4
Literature comparison of apparent activation energies and turnover frequencies (TOFs) at T = 450 °C for selected catalysts.

Metal	Catalyst	Apparent activation energy (kcal/mol)[a]			TOF (s^{-1})[a]	Reference[b]
		CH_4	CO_2	CO		
	0.5Pt	18.5	14.8	n/c	9.6[c]	This study
	Pt/SiO_2	n/c	19	n/c	0.85	[51,52]
	Pt/TiO_2	n/c	19	n/c	4.4	[51,52]
Ni	Ni/SiO_2	13	n/c	n/c	0.61	[53]
	Ni/La_2O_3	n/c	n/c	15	9.2	[49,50]
Rh	Rh/SiO_2	n/c	23	n/c	0.14	[54]
	Rh/TiO_2	n/c	18	n/c	25	[52]
Ir	Ir/SiO_2	n/c	n/c	42	0.04	[55]
	Ir/TiO_2	n/c	18	n/c	22	[52]

n/c refers to not calculated.
[a] Activation energies and TOFs as reported by Bradford and Vannice [7]. TOFs have been corrected to their standard conditions.
[b] Original references for the reported values.
[c] TOF of 3.5 s^{-1} corrected to higher partial pressures of CH_4 and CO_2 using approach of Bradford and Vannice [7], which is 0.5 order for CH_4 and 0.25 order for CO_2.

In this compilation of TOFs, most of the original studies have estimated the value based on methane conversion and the number of available metal sites from H_2 or CO chemisorption. Since methane is activated by the metal sites, it is a good assumption that the sites for methane activation at least correlate to the available metal surface area that can chemisorb these probe molecules even if it is not exactly matching. Whereas this approach is common, there is also generally a desire to use a reactant molecule to determine the number of actives sites. Since, in this study, both metallic Ni and Pt sites may activate methane (as seen in dry reforming activity for the control catalysts), basic sites that are able to adsorb acidic CO_2 was selected to determine the number of active sites for normalization of the CO_2 conversion rate. Thus, differences in TOFs could be embedded in the choice of quantifying the active sites and the selection of CO_2 or CH_4 conversion rates, though the latter is expected to be minimal because these would be equal when there are no side reactions.

The CO_2 TOF value from the present study was corrected to these conditions using the correction factors of 0.5 order for CH_4 and 0.25 order for CO_2. These are the same correction factors as used for the Ni/La_2O_3, [49,50] which is the most active sample from the literature not containing Ir or Rh. It should be noted that the present study was performed at the same temperature as the comparison whereas the Ni/La_2O_3, [49,50] was used in dry reforming at T > 450 °C and corrected to the same conditions used by Bradford and Vannice [7] for comparison purposes. From Table 4, it is evident that the catalyst used for the current study had one of the highest TOF surpassed only by Rh/SiO_2 and Ir/TiO_2.

4. Conclusion

Low temperature (430–470 °C) dry reforming of methane was studied over different metal based catalysts on a ceria–zirconia oxide support. The combination of Pt with NiMg/(Ce,Zr)O_2 catalysts increased the low temperature dry reforming activity compared to the control catalysts without Ni and Mg and Pt. The activity increase is attributed to the high dispersion and synergistic effects between the platinum and oxide phases, which is correlated to the reduction temperature and the number of basic sites. The study proposed a complex catalyst system in which a conventional reforming catalyst (NiMg/(Ce,Zr)O_2) is modified by a precious metal to balance the conversion of both reactants. As a result, high conversions were achieved at low temperatures, which is also evident in the comparison of TOFs to the literature values. Minimal deactivation occurred for the long-term testing. Further research is needed to examine the active site requirements for both CO_2 and CH_4, as well as increasing the H_2:CO ratio through the addition of steam (bi-reforming) to the feed to decrease the driving force for the rWGS reaction.

Acknowledgments

The authors gratefully acknowledge funding from Hinkley Center for Solid and Hazardous Waste Management. NHE also acknowledges the Graduate Students Success Scholarship that is administered by the USF School of Graduate Studies. The authors thank Yolanda A. Daza for her help during this project.

Appendix A. Supplementary data

Supplementary data associated with this article can be found, in the online version, at http://dx.doi.org/10.1016/j.apcatb.2015.05.021

References

[1] J.R. Rostrup-Nielsen, J. Sehested, J.K. Nørskov, Adv. Catal. 47 (2002) 65–139.
[2] S. Damyanova, B. Pawelec, K. Arishtirova, M.V.M. Huerta, J.L.G. Fierro, Appl. Catal. B: Environ. 89 (2009) 149–159.
[3] D. Baudouin, J.-P. Candy, U. Rodemerck, F. Krumeich, L. Veyre, P.B. Webb, C. Thieuleux, C. Copéret, Catal. Today 235 (2014) 237–244.
[4] A.A. Lemonidou, I.A. Vasalos, Appl. Catal. A: Gen. 228 (2002) 227–235.
[5] A. Yamaguchi, E. Iglesia, J. Catal. 274 (2010) 52–63.
[6] S. Zhang, S. Muratsugu, N. Ishiguro, M. Tada, ACS Catal. 3 (2013) 1855–1864.
[7] M. Bradford, M. Vannice, Catal. Rev. 41 (1999) 1–42.
[8] C. Song, W. Pan, Catal. Today 98 (2004) 463–484.
[9] EPA, Methane Emession, <http://www.epa.gov/climatechange/ghgemissions/gases/ch4.html/>, 2010.
[10] EPA, Landfill Methane Outreach Program, <http://www.epa.gov/lmop/publications-tools/handbook.html/>, 2011.
[11] D. Pakhare, J. Spivey, Chem. Soc. Rev. 43 (2014) 7813–7837.
[12] G. Valderrama, C. Urbina de Navarro, M.R. Goldwasser, J. Power Sources 234 (2013) 31–37.
[13] P. Kumar, Y. Sun, R.O. Idem, Energy Fuels 21 (2007) 3113–3123.
[14] N. Laosiripojana, S. Assabumrungrat, Appl. Catal. A: Gen. 290 (2005) 200–211.
[15] D.M. Walker, S.L. Pettit, J.T. Wolan, J.N. Kuhn, Appl. Catal. A: Gen. 445–446 (2012) 61–68.
[16] G. Vlaic, P. Fornasiero, S. Geremia, J. Kašpar, M. Graziani, J. Catal. 168 (1997) 386–392.
[17] J.A.C. Ruiz, F.B. Passos, J.M.C. Bueno, E.F. Souza-Aguiar, L.V. Mattos, F.B. Noronha, Appl. Catal. A: Gen. 334 (2008) 259–267.
[18] G. Balducci, J. Kašpar, P. Fornasiero, M. Graziani, M.S. Islam, J. Phys. Chem. B 102 (1998) 557–561.
[19] X.E. Verykios, Int. J. Hydrogen Energy 28 (2003) 1045–1063.
[20] W.-S. Dong, H.-S. Roh, K.-W. Jun, S.-E. Park, Y.-S. Oh, Appl. Catal. A: Gen. 226 (2002) 63–72.
[21] S. Wang, G. Lu, Ind. Eng. Chem. Res. 38 (1999) 2615–2625.
[22] M.M. Yung, S. Cheah, K. Magrini-Bair, J.N. Kuhn, ACS Catal. 2 (2012) 1363–1367.
[23] S.M. Stagg-Williams, F.B. Noronha, G. Fendley, D.E. Resasco, J. Catal. 194 (2000) 240–249.
[24] Q. Yu, W. Chen, Y. Li, M. Jin, Z. Suo, Catal. Today 158 (2010) 324–328.
[25] G. Kim, D.-S. Cho, K.-H. Kim, J.-H. Kim, Catal. Lett. 28 (1994) 41–52.
[26] M.C.J. Bradford, M.A. Vannice, Appl. Catal. A: Gen. 142 (1996) 73–96.
[27] S. Rossignol, F. Gérard, D. Duprez, J. Mater. Chem. 9 (1999) 1615–1620.
[28] J.C. Escritori, S.C. Dantas, R.R. Soares, C.E. Hori, Catal. Commun. 10 (2009) 1090–1094.
[29] S. Pengpanich, V. Meeyoo, T. Rirksomboon, K. Bunyakiat, Appl. Catal. A: Gen. 234 (2002) 221–233.
[30] C.E. Hori, H. Permana, K.Y.S. Ng, A. Brenner, K. More, K.M. Rahmoeller, D. Belton, Appl. Catal. B: Environ. 16 (1998) 105–117.
[31] K.S. Devi, S. Jayashree, React. Kinet. Mech. Catal. 108 (2013) 183–192.
[32] N. Kamiuchi, M. Haneda, M. Ozawa, Catal. Today 201 (2013) 79–84.
[33] H.-S. Roh, K.-W. Jun, W.-S. Dong, J.-S. Chang, S.-E. Park, Y.-I. Joe, J. Mol. Cat. A: Chem. 181 (2002) 137–142.
[34] L.F. Liotta, A. Macaluso, A. Longo, G. Pantaleo, A. Martorana, G. Deganello, Appl. Catal. A: Gen. 240 (2003) 295–307.
[35] F. Giordano, A. Trovarelli, C. de Leitenburg, M. Giona, J. Catal. 193 (2000) 273–282.
[36] H.-S. Roh, W.-S. Dong, K.-W. Jun, S.-E. Park, Chem. Lett. 30 (2001) 88–89.
[37] A. Goguet, F. Meunier, J.P. Breen, R. Burch, M.I. Petch, A. Faur Ghenciu, J. Catal. 226 (2004) 382–392.
[38] E. Rogemond, R. Fréty, V. Perrichon, M. Primet, S. Salasc, M. Chevrier, C. Gauthier, F. Mathis, J. Catal. 169 (1997) 120–131.
[39] V. Pitchon, J.F. Zins, L. Hilaire, G. Maire, React. Kinet. Catal. Lett. 59 (1996) 203–209.
[40] A.M. Diskin, R.H. Cunningham, R.M. Ormerod, Catal. Today 46 (1998) 147–154.
[41] P. Fornasiero, J. Kašpar, M. Graziani, J. Catal. 167 (1997) 576–580.
[42] F.B. Passos, E.R. de Oliveira, L.V. Mattos, F.B. Noronha, Catal. Today 101 (2005) 23–30.
[43] S.M. de Lima, A.M. Silva, I.O. da Cruz, G. Jacobs, B.H. Davis, L.V. Mattos, F.B. Noronha, Catal. Today 138 (2008) 162–168.
[44] X. Wu, J. Fan, R. Ran, D. Weng, Chem. Eng. J. 109 (2005) 133–139.
[45] R.C. Egeberg, S. Ullmann, I. Alstrup, C.B. Mullins, I. Chorkendorff, Surf. Sci. 497 (2002) 183–193.
[46] A. Kambolis, H. Matralis, A. Trovarelli, C. Papadopoulou, Appl. Catal. A: Gen. 377 (2010) 16–26.
[47] J. Wei, E. Iglesia, J. Phys. Chem. B 108 (2004) 4094–4103.
[48] Ş. Özkara-Aydınoğlu, A. Erhan Aksoylu, Chem. Eng. J. 215–216 (2013) 542–549.
[49] Z. Zhang, X.E. Verykios, J. Chem. Soc. Chem. Commun. (1995) 71–72. <http://pubs.rsc.org/en/Content/ArticleLanding/1995/C3/C39950000071#!divAbstract/>.
[50] Z. Zhang, X.E. Verykios, Appl. Catal. A: Gen. 138 (1996) 109–133.
[51] M.C.J. Bradford, M.A. Vannice, J. Catal. 173 (1998) 157–171.
[52] M.C. Bradford, M. Albert Vannice, Catal. Today 50 (1999) 87–96.
[53] T. Osaki, T. Horiuchi, K. Suzuki, T. Mori, Catal. Lett. 35 (1995) 39–43.
[54] M. Sigl, M.C. Bradford, H. Knözinger, M.A. Vannice, Top. Catal. 8 (1999) 211–222.
[55] A. Erdőhelyi, K. Fodor, F. Solymosi, Stud. Surf. Sci. Catal. 107 (1997) 525–530.

Update

Applied Catalysis B: Environmental
Volume 182, Issue , March 2016, Page 645

DOI: https://doi.org/10.1016/j.apcatb.2015.10.017

Applied Catalysis B: Environmental 182 (2016) 645

Contents lists available at ScienceDirect

Applied Catalysis B: Environmental

journal homepage: www.elsevier.com/locate/apcatb

Corrigendum

Corrigendum to "Low temperature dry reforming of methane over Pt–Ni–Mg/ceria–zirconia catalysts" [Appl. Catal. B: Environ. 179 (2015) 213–219]

Nada H. Elsayed, Nathan R.M. Roberts, Babu Joseph, John N. Kuhn*

Department of Chemical & Biomedical Engineering, University of South Florida, United States

The authors regret to report that the printed version of the aforementioned article contains some errors pertaining to the amount of metals loaded on the catalyst supports.

Although the reported reaction and characterization results are accurate and correct (except as follows below), the mass loadings for the metals on the catalysts were incorrectly reported resulting in the following corrections:

Table 1 Corrections.

Reported notation	Correct catalyst formulation
0.5Pt/CeZr	0.16%Pt–$Ce_{0.6}Zr_{0.4}O_2$
0Pt	$Ce_{0.6}Zr_{0.4}O_2$–1.34Ni1.00Mg
0.2Pt	0.07%Pt–$Ce_{0.6}Zr_{0.4}O_2$–1.34Ni1.00Mg
0.5Pt	0.16%Pt–$Ce_{0.6}Zr_{0.4}O_2$–1.34Ni1.00Mg
1Pt	0.33%Pt–$Ce_{0.6}Zr_{0.4}O_2$–1.34Ni1.00Mg
2Pt	0.64%Pt–$Ce_{0.6}Zr_{0.4}O_2$–1.34Ni1.00Mg

In addition, in Table 2, one of the samples' CO_2 X_{10} and X_{50} values were misstated.

Table 2 Corrections.

Reported sample	Reported X_{10} CO_2 temperature (°C)	Reported X_{50} CO_2 temperature (°C)	Correct X_{10} CO_2 temperature (°C)	Correct X_{50} CO_2 temperature (°C)
0.5Pt/CeZr	759	810	488	625

The authors would like to apologize for any inconvenience caused.

DOI of original article: http://dx.doi.org/10.1016/j.apcatb.2015.05.021.

* Corresponding author.
E-mail address: jnkuhn@usf.edu (J.N. Kuhn).

http://dx.doi.org/10.1016/j.apcatb.2015.10.017